

**Modelling low dimensional nanostructures,  
their thermo-electromechanical properties and applications in  
engineering, physical and biological sciences**

**Melnik, R.V.N. and Patil, S.**

**In: Proceedings of the International Scientific Conference, Simulation-2010,  
May 12-14, 2010, NASU, Institute for Modeling in Energy Engineering,  
Vol. 1, pp. 60-72, 2010.**

==

**Part of the Collection of Scientific Works “MODELING AND INFORMATION  
TECHNOLOGIES”, UDK 621.396+681.511, ISSN 2309-7647**

The publication reflects new aspects of the simulation of complex technical systems, theoretical issues of electrical engineering, informatics, algorithms for solving problems of automation of technological processes, the construction of computing devices and systems, information security in computing systems and networks. It is intended for researchers who are involved in the design of complex systems.

**Special Issue of the Collection of Scientific Works  
“Modeling and Information Technologies”:  
Materials of the the International Scientific Conference, Simulation-2010  
(May 12 - 14, 2010).**

**Publisher: NASU, Institute for Modeling in Energy Engineering, 2010.**

==

R.V.N. Melnik, Ph.D. and S. Patil, PhD  
M2NeT Lab, Wilfrid Laurier University,  
75 University Avenue West, Waterloo,  
ON, Canada N2L 3G5

## **MODELLING LOW DIMENSIONAL NANOSTRUCTURES, THEIR THERMO-ELECTROMECHANICAL PROPERTIES AND APPLICATIONS IN ENGINEERING, PHYSICAL AND BIOLOGICAL SCIENCES**

**Abstract.** We consider the problem of simulating and predicting properties of low dimensional nanostructures that are becoming increasing important in many applications ranging from optoelectronics to biology. For quite some time, both strain and piezoelectric effects have been used as tuning parameters in controlling properties such structures. However, thermal effects have been largely neglected. In this contribution, by using the fully coupled model of thermoelectroelasticity, we build on our previous results in analyzing the influence of these effects on properties of low dimensional nanostructures, focusing on quantum dots.

**1. Introduction.** Engineering and physical sciences are abundant of current and potential applications of low dimensional nanostructures, including nanowires and quantum dots. Furthermore, such nanostructures found a wide range of applications in biological science and medicine and they are becoming more and more common in these fields too. For example, quantum dots have been in comparative embryology, for imaging many phenomena within the nuclei of living cells, as well as limitless applications in all other areas of biology. In order to use such nanostructures in applications ranging from solar panels to tailoring them to track specific chemical reactions inside nuclei, such as how proteins help repair DNA after irradiation we need to be able to predict their properties.

Wide band gap semiconductors have attracted much attention due to their potential applications in short wavelength optoelectronic devices. Currently, III-V GaN-based materials are leading materials for the fabrication of blue-green light emitting devices [1]. However, GaN-based low dimensional structures are found to have relatively high carrier densities to generate optical gain. This is due to the giant internal electric field as a result of misfit-strain induced piezoelectric and spontaneous polarization effects [2, 3]. To resolve higher carrier density problem in generating optical gain, II-VI ZnSe and CdTe-based nanostructures are the leading alternatives [4]. Recent advances in growth technologies of II-VI semiconductors now permit to grow high quality heterostructures [5]. Thus, with current progress in II-VI semiconductors, corresponding theoretical studies become very important. Among II-VI semiconductors, the CdTe/ZnTe system has become particularly interesting due to its potential to operate in the green region of spectrum and serve as an alternative to GaN-based systems [1, 6, 7].

In term of biological applications, Cd-based nanstructures are important potential building blocks in bio-nanotechnological and bio-medicine applications. However, it is critical to better understand properties of such nanostructures in these fields in particular. Firstly, it is well-known that making good quantum dots for biological research is a very complex process. Secondly, Cd itself is toxic, and the compound also can oxidize easily, so the nanocrystals must often be encapsulated in a protective shell which makes the entire analysis even more complex.

In what follows, we formulate a 3D strongly coupled thermopiezoelectric model for zincblende (ZB) nanocrystals and pay our major attention to the thermal loading effect on piezoelectric properties and its influence on the optoelectronic properties of the CdTe QWR embedded in ZnTe matrix. Next, we analyze the difference between properties of quantum wires and quantum dots based on the models combining quantum and classical effects for nanstructures with cylindrical geometries.

**2. Mathematical models for nanostructures accounting for coupled thermoelectromechanical effects.** We start our discussion with the goal to simulate quantum nanowires accounting for such classical effects as piezoeffect, strain, as well as thermal effects. In what follows, we formulate a general mathematical model, combining classical and quantum mechanical parts, following the ideas and discussion originally proposed in [8]. This three dimensional model has been developed with coupled multi-physics governing equations.

**2.1 Classical part.** The 3D linear fundamental equations for the thermoelectromechanical body (such as a nanostructure considered later in Section 3) occupying volume  $\Omega$ , under steady state conditions, in our case can be summarized as follows [9, 10]:

$$\begin{aligned} \nabla \bullet \sigma &= F, \\ \nabla \bullet D &= q, \end{aligned} \tag{1}$$

where  $\sigma$  is the stress tensor and  $D$  is the electric displacement vector,  $F$  and  $q$  are mechanical body force and electric charge in  $\Omega$ , respectively. Note that, at the thermal equilibrium, the temperature change becomes spatially independent and the problem is governed by the equations (1) only. Equations (1) are coupled and the coupling is given by the explicit forms of constitutive relations relating thermoelectromechanical quantities. For, ZB nanostructures (zinc-blende, that is those with cubical symmetry) in cartesian coordinates these relations are given as follows:

$$\begin{aligned}
\sigma_{xx} &= c_{11}\epsilon_{xx} + c_{12}\epsilon_{yy} + c_{12}\epsilon_{zz} - \beta_1 T \\
\sigma_{yy} &= c_{12}\epsilon_{xx} + c_{11}\epsilon_{yy} + c_{12}\epsilon_{zz} - \beta_2 T \\
\sigma_{zz} &= c_{12}\epsilon_{xx} + c_{12}\epsilon_{yy} + c_{11}\epsilon_{zz} - \beta_3 T \\
\sigma_{xy} &= 4c_{44}\epsilon_{xy} - e_{14}E_z, \quad \sigma_{yz} = 4c_{44}\epsilon_{yz} - e_{14}E_x \\
\sigma_{zx} &= 4c_{44}\epsilon_{zx} - e_{14}E_y, \quad D_x = e_{14}\epsilon_{yz} + \chi_{11}E_x \\
D_y &= e_{14}\epsilon_{zx} + \chi_{11}E_y, \quad D_z = e_{14}\epsilon_{xy} + \chi_{33}E_z.
\end{aligned} \tag{2}$$

Here  $c_{ij}$ ,  $e_{ij}$ ,  $\chi_{ij}$  and  $\beta_i$  are elastic moduli, piezoelectric constants, dielectric constants and stress-temperature material constants, respectively,  $\epsilon$ ,  $E$  and  $T$  are strain tensor, electric field and temperature, respectively.

We remark that in many cases simulations of nanowires can be performed with the above model reduced to a 2D formulation. However, piezoelectric coupling, which appears through shear components in ZB crystals [11] requires to solve this problem using a 3D model.

**2.2. Quantum part.** Classical properties in low dimensional nanostructures are intrinsically interwoven with quantum (electronic) properties. The quantum mechanical part of our model, which we next use for simulating CdTe/ZnTe QWRs, is based on the Schrödinger equation for single conduction band. The important point to realize is that the thermopiezoelectric effects (that is classical effects described in Section 2.1) will modify the potential energy term. In our particular situation, the Schrödinger equation and effective potential are given as follows (electron is considered as a particle with effective mass  $m_e^*$  experiencing effective potential,  $V_c$ ):

$$\begin{aligned}
\nabla \bullet \left\{ -\frac{\hbar^2}{2m_e^*} \nabla \psi \right\} + V_c \psi &= E \psi, \\
V_c &= r \cdot E_g + a_c (\epsilon_{xx} + \epsilon_{yy} + \epsilon_{zz}) - eV - \frac{\alpha_T T^2}{\beta_T + T},
\end{aligned} \tag{3}$$

where  $\psi$  is the wave function and  $E$  is corresponding eigenvalue,  $r$ ,  $a_c$  and  $e$  are band offset ratio, conduction band deformation potential and electronic charge respectively,  $E_g$  and  $V$  are the band gap and electric potential respectively,  $\alpha_T$  and  $\beta_T$  are the Varshni coefficients [12].

The physical parameters used in this calculation are given in Table 1.

**Table 1** Physical parameters used for calculations.

Material constants	CdTe	ZnTe
$c_{11}$ (GPa)	53.8*	72.2**
$c_{12}$ (GPa)	37.4*	40.9**
$c_{44}$ (GPa)	20.18*	30.8**
$\epsilon_{14}$ (C/m <sup>2</sup> )	0.084[13]	0.028[14]
$\chi_{11}$	10.4[15]	10.3[16]
$\beta_1$ (Pa/K)	97205.65+	-73220.34+
$r$	0.75^	0.25^
$a_c$ (eV)	-1.8^	-3.5^
$E_g$ (eV)	1.606^	2.394^
$\alpha_T$ (eV/K)	0.4357e-3[12]	0.467e-3[17]
$\beta_T$ (K)	183.3[12]	168[17]

(see [8] for notations on references and more details).

**3. Simulating quantum wire properties.** Based on the model highlighted in the previous section, we carry out simulations by using the finite element method. The domain is meshed with quadratic triangular elements and the resulting algebraic eigenvalue problem is solved numerically overcoming known difficulties [18]. A rectangular CdTe QWR of dimensions 10x10x70nm is embedded in the 40x40x150nm ZnTe barrier. The lattice mismatch in CdTe/ZnTe QWR is  $\epsilon_0 = 5.89\%$ .

Following [8], we recall that the magnitude of strain component  $\epsilon_{xx}$  is observed to be less than about 3.45% ( $\sim \epsilon_0/2$ ) at all points inside the QWR, except for the region near the edges where the strain has higher magnitude than  $\epsilon_0/2$ . The QWR causes the surrounding matrix to become strained and the strain decays slowly to zero away from the QWR. We also note that the magnitude of the hydrostatic strain component is particularly important as it leads to the rigid shift in electronic band structure [19] and we refer the interested reader to [8] on particular numerical values in this case. Figure 1 shows electric potential and x-component of electric field in the x-y plane. As we pointed out in [8], the potential difference across the QWR ends is  $\sim 0.08$  V, which is smaller by order of magnitude as compared to GaN ( $\sim 2$  V) [20]. Also, the magnitude of the electric field exceeds 5 MV/m near the edges of the QWR and has the magnitude in fractions of MV/m inside the QWR. This is again a very small magnitude of electric field as compared to GaN ( $\sim 600$  MV/m) [20].

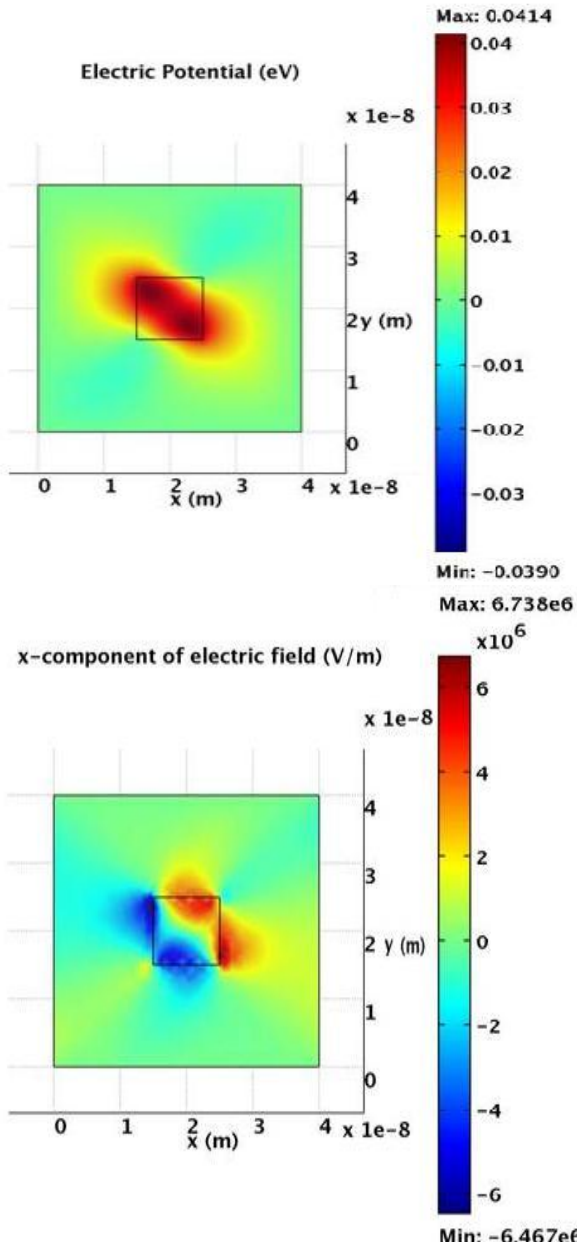
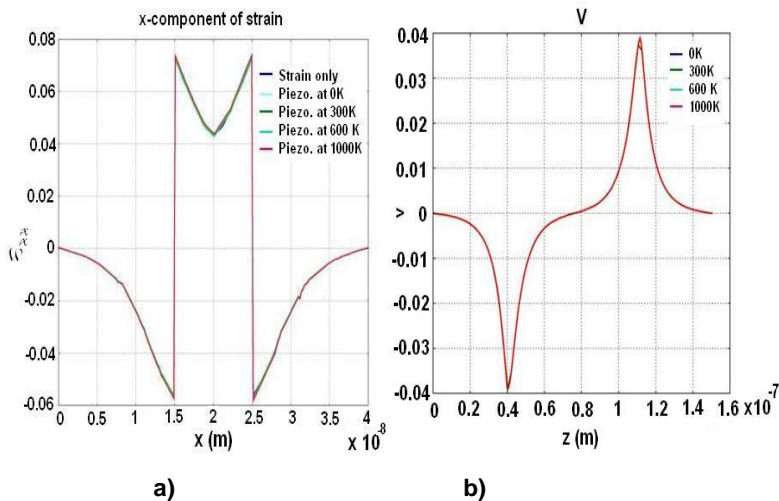


**Figure 1:** Electric potential (upper) and x-component of electric field in x-y plane (lower).

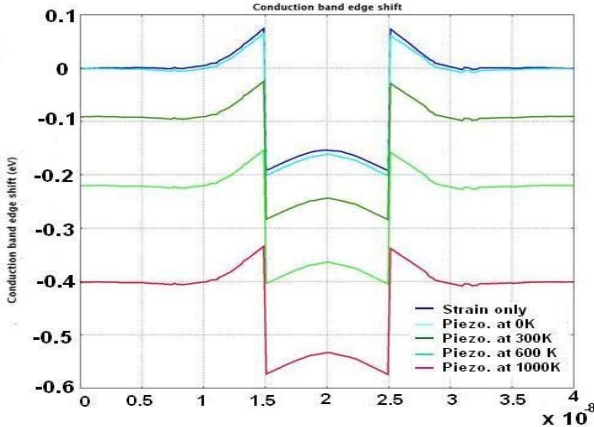
The smaller magnitudes of electric potential and electric field represent an advantage of CdTe based nanostructures over GaN as the latter structures face a problem of higher carrier density for generating optical gain.

Figure 2 shows a)  $\epsilon_{xx}$  along x direction and b) electric potential along z-direction as a function of thermopiezoelectric effects. The electromechanical parameters for the CdTe/ZnTe system are relatively less sensitive to temperature than those of GaN/AlN. This can be attributed to the low values of stress-temperature coefficients and relatively weak electromechanical coupling in CdTe/ZnTe compared to the GaN/AlN system. This also provides an added advantage to CdTe/ZnTe over GaN based nanostructures related to the thermal stability of piezoelectric quantities which may result in more stable optical properties.

Figure 3 shows the conduction band edge shifts in the CdTe/ZnTe QWR vs thermal loadings from 0 K to 1000 K.



**Figure 3:** a)  $\epsilon_{xx}$  and b) electric potential as a function of thermopiezoelectric effects



**Figure 3:** Conduction band edge shifts against thermal loadings

The conduction band edge shifts at lower temperature are positive ( $\sim 7$  meV at 0 K inside the QWR), indicating an increase in effective band gap. However, as temperature increases band gap shifts become negative ( $\sim -55$  meV at 1000K inside the QWR). The band gap shifts range from blue shift at low temperature to red shift at higher temperatures. The band gap shifts take peak values at the edges. In the ZnTe matrix, outside the QWR, conduction band edge shifts show similar trends. The conduction band edge shift at the operating temperature of 300 K is small ( $\sim 27$  meV). Hence, we conclude that the CdTe/ZnTe QWR system is more stable with respect to thermopiezoelectric effects compared to other similar materials such as GaN.

Finally, as it was pointed out in [8], the ground state eigenvalue without any electromechanical loading for CdTe/ZnTe is 0.203 eV which further decreases to 0.2025 eV and 0.197 eV with incorporation of strain and piezoelectric effects, respectively. This change in ground state eigenvalues may lead to change of optoelectronic properties.

**4. Simulating quantum dots and comparisons.** Now, we aim at comparisons of the properties of quantum nanowires and quantum dots. In this discussion, we follow closely [21] (and our recent presentation at the SPIE conference; here and further we refer to it generically as [21]). We consider cylindrical QDs and QWs which are axisymmetric around z-axis. Now we are considering a more difficult situation of wurtzite (WZ) nanotubes which have hexagonal crystalline lattice. They are axisymmetric, and therefore the solution of the model is axisymmetric as well. The material constants for the crystal with WZ symmetry used in this work are given in [21]. In this case, the original three-dimensional problem, formulated in Section 2, can be reduced to a simpler two-dimensional problem. In this case, equations (1) have the following form:

$$\frac{\partial \sigma_{rr}}{\partial r} + \frac{\partial \sigma_{rz}}{\partial z} + \frac{\sigma_{rr} - \sigma_{\theta\theta}}{r} = 0, \quad \frac{\partial \sigma_{rz}}{\partial r} + \frac{\partial \sigma_{zz}}{\partial z} + \frac{\sigma_{rz}}{r} = 0, \quad \frac{\partial D_r}{\partial r} + \frac{\partial D_z}{\partial z} + \frac{D_r}{r} = 0.$$

(2)

These equations are invariant with respect to rotations around the  $z$ -axis, hence solutions can be separated into a  $(r, z)$  part and a  $\theta$  part, subject to adequate boundary conditions. The constitutive relations then take the following form for WZ nanostructures:

$$\begin{aligned}\sigma_{rr} &= C_{11}\varepsilon_{rr} + C_{12}\varepsilon_{\theta\theta} + C_{11}\varepsilon_{zz} - e_{31}E_z - \beta_1\Theta, & \sigma_{rz} &= C_{44}\varepsilon_{rz} - e_{15}E_r, \\ \sigma_{zz} &= C_{13}\varepsilon_{rr} + C_{13}\varepsilon_{\theta\theta} + C_{33}\varepsilon_{zz} - e_{33}E_z - \beta_3\Theta, & D_r &= e_{15}\varepsilon_{rz} - \epsilon_{11}E_r \\ D_z &= e_{31}\varepsilon_{rr} + e_{31}\varepsilon_{\theta\theta} + e_{33}\varepsilon_{zz} - \epsilon_{33}E_z + p_3\Theta + P_z^{SP}.\end{aligned}$$

(3)

One important moment to note is that based on the total differential of the general thermodynamic potential with Taylor series expansion of differentials of electromechanical quantities a generalization of Eq. (3) to the nonlinear case can be derived [21]. To take into account the lattice mismatch by the corresponding expressions for the strain tensor components with  $\varepsilon_a = (a_m - a_Q)/a_Q$  and  $\varepsilon_c = (c_m - c_Q)/c_Q$  inside the QD and QW. Quantities  $a_m$ ,  $c_m$  and  $a_Q$ ,  $c_Q$  are the lattice constants of the matrix and the QD/QW, respectively, while quantities  $\varepsilon_a$  and  $\varepsilon_c$  are the local intrinsic strains (lattice mismatch) along the  $a$  and  $c$  directions, respectively. The directions  $a$  and  $c$  correspond to the shorter and longer dimensions of the unit cell of the wurtzite crystal, respectively. The hydrostatic strain component is given by

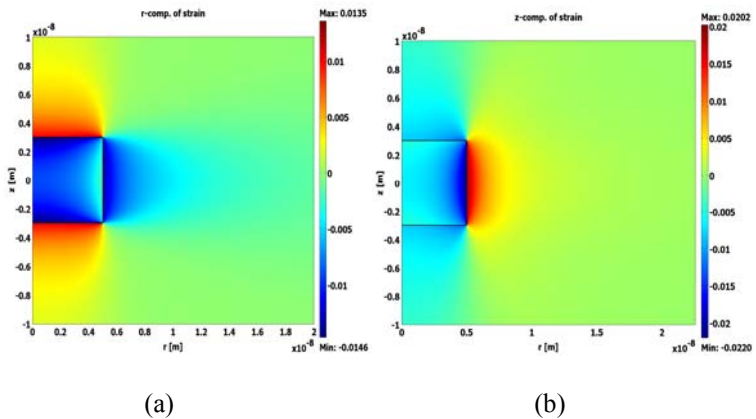
$$\varepsilon_{vol} = \varepsilon_{rr} + \varepsilon_{zz} + \varepsilon_{\theta\theta}$$

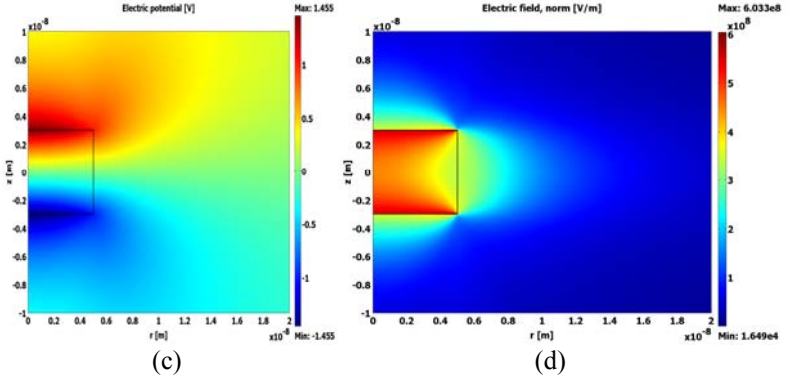
As we pointed out before, the hydrostatic strain component is particularly important due to the fact that it provides information about rigid shift in energy subbands. In the plane stress case, by applying a 2D analytical method, it can be defined as in [21].

As we discussed in [21], the per cent misfit strain in the case of the GaN/AlN system is -2.47% and -4.07% in  $a$  and  $c$  directions, respectively. We assume that the QDs and QWs are oriented such that the  $c$ -direction of the crystal is along the  $z$ -axis. As the substrate is relatively large compared to the QD, we follow common practice to neglect lattice mismatch inside the matrix. The electromechanical parameters used in the calculations are given in [21]. All our numerical experiments have been performed under the condition for the relative errors between successive refinements to be less than  $10^{-7}$ . In our case it has been achieved with around  $10^6$  triangular elements. Numerical solutions reflect the effect of the decreasing computational error when the solution approaches the boundary of the domain. Results originally obtained based on the development stemming from [21] clearly depict this feature, as highlighted in Figures 4, 5, and 6.

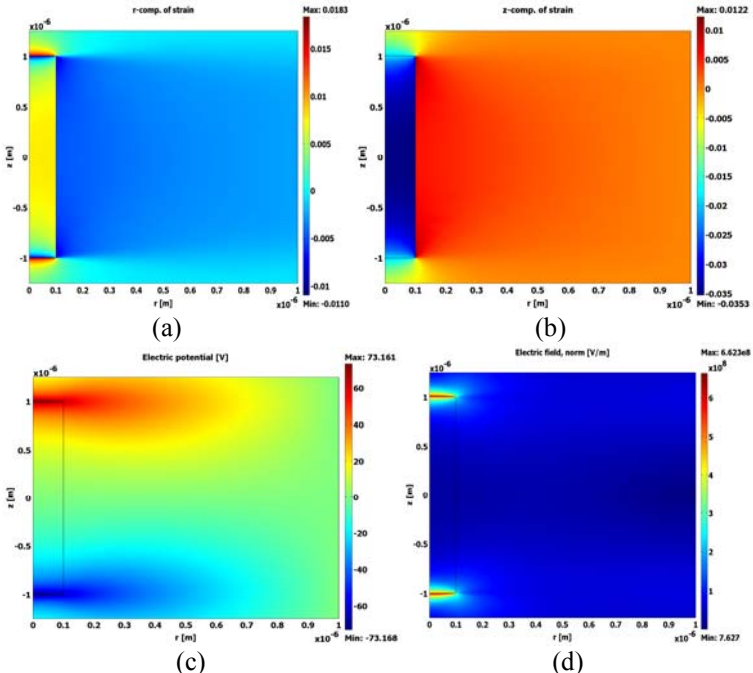
The focus we give here is on WZ GaN/AlN QD systems. Dirichlet boundary conditions are imposed along three boundaries, while other conditions are taken the same as we took earlier (see the above quoted papers). In this case, due to the axisymmetry of the system (equations, geometry and boundary conditions) there is no angular dependence. In what follows, we highlight results of [21] for the QD is of radius 5nm and of height 10 nm and the QW is 2 micron long and has radius of 100 nm.

Figure 4 shows the electromechanical distributions in QD at 300K. Fig. 4 a) and 4 b) show distributions of  $\varepsilon_{rr}$  and  $\varepsilon_{zz}$  in  $r$ - $z$  plane, respectively. The magnitude of both the strain components,  $\varepsilon_{rr}$  and  $\varepsilon_{zz}$ , is observed to be less than about 1% and 2%, respectively, at all points inside the QD, except for the region near the edges where the strain has higher magnitude.  $\varepsilon_{rr}$  has its highest magnitude at the centre of the QD however  $\varepsilon_{zz}$  has it at the edge in  $r$ -direction. The QD causes the surrounding matrix to become strained and the strain decays slowly to zero away from the QWR. Thus strain relaxation occurs over most of the QD area. The electric potential (Fig. 4c), develops across the top and bottom of the QD,i.e. along  $z$ -direction and has a magnitude of  $\sim 2.9V$ . As a result of this, electric field is seen to have highest magnitude at the centre of the QD. The highest magnitude of electric field is  $\sim 6 \times 10^8 V/m$ . Our results agree well with previous reports (see [21] and references therein).





**Figure 4:** The electromechanical distributions in QD at 300K. a) r-component of strain b) z-component of strain, c) electric potential d) electric field.



**Figure 5:** The electromechanical distributions in QW at 300K. a) r-component of strain b) z-component of strain, c) electric potential d) electric field.

Figure 5 shows the electromechanical distributions in QW at 300K. Fig. 5 a) and 5 b) show distributions of  $\epsilon_{rr}$  and  $\epsilon_{zz}$  in  $r$ - $z$  plane, respectively. In contrast to

the QD  $\varepsilon_{rr}$  has its lowest magnitude at the centre of the QW and  $\varepsilon_{zz}$  has it at the centre. Due to relatively large structure, significant strain relaxation occurs over most of the wire area. However, the electric potential (Fig. 5c), develops across the top and bottom of the QD,i.e. along z-direction. As a result of this, electric field is seen to have lowest magnitude at the centre of the QD dn has higher magnitudes near the top and bottom edges. The highest magnitude of electric field is slightly higher than that of QD, i.e.  $\sim 6.6 \times 10^8$  V/m.

Figure 6 shows the effect of temperature on electromechanical quantities for the cylindrical GaN/AlN QDs. Inside the QD, the magnitude of  $\varepsilon_{rr}$  (along the z-axis at  $r = 0$ , figure 6(a)) decreases with an increase in temperature. At the center of the QD the magnitudes are  $\sim 0.8\%$  at 300 K and  $\sim 0.6\%$  at 700 K. The magnitude of  $\varepsilon_{rr}$  decreases towards zero (unstrained region) faster at higher temperature than at lower temperature. As seen from figure 6(b),  $\varepsilon_{zz}$  is negative everywhere for all temperatures. The magnitude of  $\varepsilon_{zz}$  at the centre of the QD, i.e. at  $z = 0$ , is  $\sim 0.67\%$  at 300 K, which increases with an increase in temperature to  $\sim 0.85\%$  at 700 K. Note that as it was observed in [21], the potential difference across the top and bottom of the QD decreases with an increase in temperature, from 2.9 V at 300 K to 2.8 V at 700 K. These and other results at 300 K are in excellent agreement with theoretical and experimental reports (see [21] and references therein).

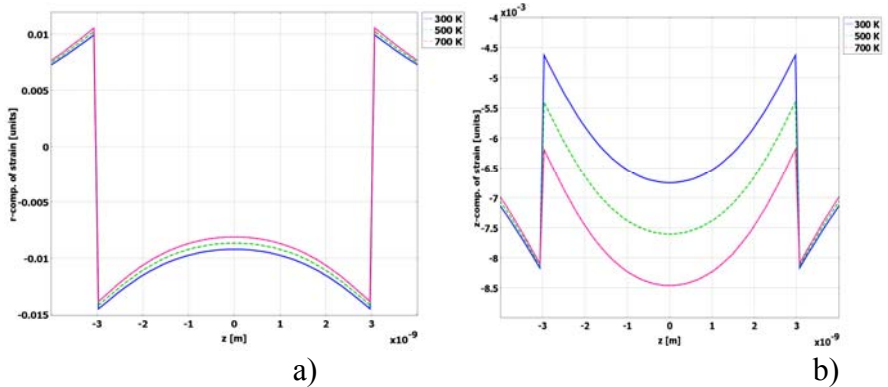


**Figure 6:** Effect of temperature on electromechanical quantities for cylindrical GaN/AlN QDs, (a) Strain,  $\varepsilon_{rr}$  , (b) strain,  $\varepsilon_{zz}$  .

Table 1. Electromechanical parameters values in QD and QW at 300K at  $r=z=0$ .

	QD		QWR	
	300K	700K	300K	700K
r-comp. of strain [%]	0.8	0.6	0.7	0.8
z-comp. of strain [%]	0.67	0.85	0.35	0.34
Electric field [ $\times 10^8$ V/m]	4.5	4.7	0.25	0.25

Recently we compile a table, presented at the SPIE, which we highlight here. From Table 1, it can be seen that electromechanical parameters are less sensitive in the case of QWs as compared to QD. This is due to the large area available for electromechanical relaxation. Hence, we conclude that the QW system is more stable with respect to thermopiezoelectric effects compared to QD. An order of magnitude smaller electric field observed in QWs as compared to QD, signifies that the QWs will require less amount of carrier concentration in order to generate optical gain. The smaller magnitudes of electric potential and electric field represent an advantage of CdTe based nanostructures over GaN as the latter structures face a problem of higher carrier density for generating optical gain [2].

**3 Conclusions.** In this contribution, we discussed the applications of a fully coupled model consisting of two parts, classical and quantum mechanical. We surveyed recent results in two areas. First, we applied our model for simulating CdTe/ZnTe quantum wires accounting for thermo-electromechanical properties. Our observations led us to conclude that thermally less sensitive electromechanical properties of CdTe/ZnTe may lead to thermally more stable performance which is important in preserving superior optoelectronic properties of nanostructures. The influence of thermal loadings on electromechanical properties of LDSNs was analyzed in detail for both two wide classes of low dimensional nanostructures, quantum wires and quantum dots. The latter has been our second area of focus. We demonstrated and emphasized that the electromechanical properties vary noticeably with temperature. In addition, we pointed out QDs are relatively more sensitive to the temperature as compared to the QWs. An order of magnitude smaller electric field observed in QWs as compared to QD, signifies that the QWs will require less amount of carrier concentration in order to generate optical gain. The results indicate that QWs have advantages over their QD counterparts, in particular with respect to the carrier density in generating optical gain. Thermally less sensitive electromechanical properties of CdTe/ZnTe may lead to thermally more stable performance which is important in preserving superior optoelectronic properties of nanostructures.

**Acknowledgements** This work, conducted in the M<sup>2</sup>NeT Laboratory (<http://www.m2netlab.wlu.ca>), was made possible by the facilities of the SHARCNET.

## References.

1. *J.T. Woo et al.*, Strain distributions and electronic subband energies of self-assembled CdTe quantum wires grown on ZnTe buffer layers. *J. Appl. Phys.* – 2007 – 102 – Art. 033521.
2. *F. Bernardini, V. Fiorentini and D. Vanderbilt*, Spontaneous polarization and piezoelectric constants of III-V nitrides. *Phys. Rev. B* – 1997 – 56 – pp. 10024-10027.

3. *M. Willatzen et al*, Dynamic coupling of piezoelectric effects, spontaneous polarization, and strain in lattice-mismatched semiconductor quantum-well heterostructures. *J. Appl. Phys.* – 2006 - 100 – Art. 024302.
4. *M. V. Maksimov et al*, Calculation of the size-quantization levels in starined ZnCdSe/ZnSe quantum wells. *Semiconductors* – 1997 – 31 – pp. 800-803.
5. *C. Onodera, T. Shoji, Y. Hiratake and T. Taguchi*, Effect in changes of conduction and valence band offsets on exciton binding energy in Cd<sub>x</sub>Zn<sub>1-x</sub>Se/ZnSySe<sub>1-y</sub> single quantum wells. *Jpn. J. Appl. Phys.* - 2007 - 46 – pp. 248-250.
6. *T. W. Kim et al*, Formation and electron activation energy of self-assembled CdTe quantum wires grown on ZnTe buffer layers. *Appl. Phys. Lett.* – 2003 – 83 – pp. 4235-4237.
7. *E. E. Onishchenko et al*, Optical spectroscopy of CdTe/ZnTe quantum-dot superlattices. *Physica E* – 2005 – 26 – pp. 153-157.
8. *S.R. Patil and R.V.N. Melnik*, Thermopiezoelectric effects on optoelectronic properties of CdTe/ZnTe quantum wires. *Physica Status Solidi (a)* – 2009 – 206 – pp. 960-964.
9. *R. V. N. Melnik*, Computational analysis of coupled physical fields in piezothermoelastic media. *Comput. Phys. Commun.* – 2001 – 142 – pp. 231-237.
10. *R. V. N. Melnik*, Modelling coupled dynamics: Piezoelectric elements under changing temperature conditions. *Int. Commun. Heat Mass Transfer.* – 2003 – 30 – pp. 83-92.
11. *R. Melnik and R. Mahapatra*, Coupled effects in quantum dot nanostructures with nonlinear strain and bridging modelling scales. *Comput. and Struct.* – 2007 – 85 – pp. 698-711.
12. *U. Pal et al*, Near band gap photoreflectance studies in CdTe, CdTe:V and CdTe:Ge crystals. *Mater. Sci. and Eng. B* – 1996 – 42 – pp. 297-301.
13. *J. Baars and F. Sorger*, Reststrahlen spectra of HgTe and Cd<sub>x</sub>Hg<sub>1-x</sub>. *Solid State Commu.* – 1972 – 10 – pp. 875-876.
14. *H. D. Riccius*, Infrared lattice vibrations of zinc selenide and zinc telluride. *J. Appl. Phys.* – 1968 – 39 – pp. 4381-4382.
15. *M. B. Kanoun et al*, Zinc-blende AlN and GaN under pressure: structural, electronic, elastic and piezoelectric properties. *Semicond. Sci. Tech.* – 2004 - 19 – pp. 1220-1231.
16. *D. Berlincourt, L. R. Shiozawa, H. Jaffe*, Electrostatic properties of sulfides, selenides, and tellurides of zinc and cadmium. *Physical Review* -1963 - 129 (3) – pp. 1009-1010.
17. *R. Passler et al*, Temperature dependence of exciton peak energies in ZnS, ZnSe, and ZnTe epitaxial films. *J. Appl. Phys.* – 1999 – 86 – pp. 4403-4411.
18. *R. V. N. Melnik*. Topological analysis of eigenvalues in engineering computations. *Eng. Computations* – 2000 – 17 – pp. 386-416.
19. *J. R. Downes, D. A. Faux, and E. P. O'Reilly*, Influence of strain relaxation on the electronic properties of buried quantum wells and wires. *Mater. Sci. and Eng., B* – 1995 - 35 – pp. 357-363.
20. *D. P. Williams, A. D. Andreev and E. P. O'Reilly*, Dependence of exciton energy on dot size in GaN/AlN quantum dots. *Phys. Rev., B* – 2006 – 73 – Art. 241301.
21. *S.R. Patil and R.V.N. Melnik*, Thermoelectromechanical effects in quantum dots. *Nanotechnology* – 2009 – 12 – Art. 125402.

directives are a fixed part of the compilation system and cannot be changed. In all these cases the programmer would like to have a tool which transforms his code in a specified and programmable way without deeply changing the original source code. Self defined directives which are treated as comments in the programming language could help him to annotate properties of the algorithmic parts.

To overcome these limitations we are defining and writing a tool which allows for implementation of the necessary rules in a transformation program. A user himself or a specialist write transformation programs for that tool and the user is applying these transformations by influencing these by setting self defined directives in his application program. This transformation tools is to be understood as a separate programming language understanding the transformation programs and transforming the application program in a new transformed program which is compiled and linked in the usual way. The transformed program is written in the original programming language and still portable and understandable.

The transformation tool provides special intrinsic data types for that purpose as strings, program segments, program names and structures, some adapted control constructs as loops run over program units as procedures, variables, statements and others, branching constructs, library calls for parsing the application programming language and structures to handle the necessary information and constructs allowing the definition and insertion of new statements in the application code. Input and output mechanisms enable the reading and writing of application codes and the output of the progress of the transformation especially for debugging. The application language used is Fortran 95. We will give an overview on the features of the mechanism and some examples.

**1. Introduction.** Engineering and physical sciences are abundant of current and potential applications of low dimensional nanostructures, including nanowires and quantum dots. Furthermore, such nanostructures found a wide range of applications in biological science and medicine and they are becoming more and more common in these fields too. For example, quantum dots have been in comparative embryology, for imaging many phenomena within the nuclei of living cells, as well as limitless applications in all other areas of biology. In order to use such nanostructures in applications ranging from solar panels to tailoring them to track specific chemical reactions inside nuclei, such as how proteins help repair DNA after irradiation we need to be able to predict their properties.

Wide band gap semiconductors have attracted much attention due to their potential applications in short wavelength optoelectronic devices. Currently, II-VI GaN-based materials are leading materials for the fabrication of blue-green light emitting devices [1]. However, GaN-based low dimensional structures are found to have relatively high carrier densities to generate optical gain. This is due to the giant internal electric field as a result of misfit-strain induced piezoelectric and spontaneous polarization effects [2, 3]. To resolve higher carrier density problem in generating optical gain, II-VI ZnSe and CdTe-based nanostructures are the leading alternatives [4]. Recent advances in growth technologies of II-VI semiconductors now permit to grow high quality heterostructures [5]. Thus, with current progress in II-VI semiconductors, corresponding theoretical studies become very important. Among II-VI semiconductors, the CdTe/ZnTe system has become particularly interesting due to its potential to operate in the green region of spectrum and serve as an alternative to GaN-based systems [1, 6, 7].

In term of biological applications, Cd-based nanostructures are important potential building blocks in bio-nanotechnological and bio-medicine applications. However, it is critical to better understand properties of such nanostructures in these fields in particular. Firstly, it is well-known that making good quantum dots for biological research is a very complex process. Secondly, Cd itself is toxic, and the compound also can oxidize easily, so the nanocrystals must often be encapsulated in a protective shell which makes the entire analysis even more complex.

In what follows, we formulate a 3D strongly coupled thermopiezoelectric model for zincblende (ZB) nanocrystals and pay our major attention to the thermal loading effect on piezoelectric properties and its influence on the optoelectronic properties of the CdTe QWR embedded in ZnFe matrix. Next, we analyze the difference between properties of quantum wires and quantum dots based on the models combining quantum and classical effects for nanostructures with cylindrical geometries.

**2. Mathematical models for nanostructures accounting for coupled thermoelectromechanical effects.** We start our discussion with the goal to simulate quantum nanowires accounting for such classical effects as piezoeffect, strain, as well as thermal effects. In what follows, we formulate a general

R.V.N. Melnik, Ph.D. and S. Patil, PhD, M2Net Lab, Wilfrid Laurier University,  
75 University Avenue West, Waterloo, ON, Canada N2L 3C5

## MODELLING LOW DIMENSIONAL NANOSTRUCTURES, THEIR THERMO-ELECTROMECHANICAL PROPERTIES AND APPLICATIONS IN ENGINEERING, PHYSICAL AND BIOLOGICAL SCIENCES

**Abstract.** We consider the problem of simulating and predicting properties of low dimensional nanostructures that are becoming increasing important in many applications ranging from optoelectronics to biology. For quite some time, both strain and piezoelectric effects have been used as tuning parameters in controlling properties such structures. However, thermal effects have been largely neglected. In this contribution, by using the fully coupled model of thermoelectroelasticity, we build on our previous results in analyzing the influence of these effects on properties of low dimensional nanostructures, focusing on quantum dots.

mathematical model, combining classical and quantum mechanical parts, following the ideas and discussion originally proposed in [8]. This three dimensional model has been developed with coupled multi-physics governing equations

**2.1 Classical part.** The 3D linear fundamental equations for the thermoelectromechanical body (such as a nanostructure considered later in Section 3) occupying volume  $\Omega$ , under steady state conditions, in our case can be summarized as follows [9, 10]

$$\begin{aligned} \nabla \cdot \sigma &= F, \\ \nabla \cdot D &= q, \end{aligned} \quad (1)$$

where  $\sigma$  is the stress tensor and  $D$  is the electric displacement vector,  $F$  and  $q$  are mechanical body force and electric charge in  $\Omega$ , respectively. Note that, at the thermal equilibrium, the temperature change becomes spatially independent and the problem is governed by the equations (1) only. Equations (1) are coupled and the coupling is given by the explicit forms of constitutive relations relating thermoelectromechanical quantities. For, ZB nanostructures (zinc-blende, that is those with cubical symmetry) in cartesian coordinates these relations are given as follows:

Here  $c_{ij}$ ,  $e_j$ ,  $\chi_{ij}$  and  $\beta_i$  are elastic moduli, piezoelectric constants, dielectric constants and stress-temperature material constants, respectively,  $\varepsilon$ ,  $E$  and  $T$  are strain tensor, electric field and temperature, respectively.

We remark that in many cases simulations of nanowires can be performed with the above model reduced to a 2D formulation. However, piezoelectric coupling, which appears through shear components in ZB crystals [11] requires to solve this problem using a 3D model.

$$\begin{aligned} \sigma_{xx} &= c_{11}\varepsilon_{xx} + c_{12}\varepsilon_{yy} + c_{12}\varepsilon_{zz} - \beta_1 T \\ \sigma_{yy} &= c_{12}\varepsilon_{xx} + c_{11}\varepsilon_{yy} + c_{12}\varepsilon_{zz} - \beta_2 T \\ \sigma_{zz} &= c_{12}\varepsilon_{xx} + c_{12}\varepsilon_{yy} + c_{11}\varepsilon_{zz} - \beta_3 T \\ \sigma_{xy} &= 4c_{44}\varepsilon_{xy} - c_{14}E_x, \quad \sigma_{yz} = 4c_{44}\varepsilon_{yz} - c_{14}E_y \\ \sigma_{zx} &= 4c_{44}\varepsilon_{zx} - c_{14}E_z, \quad D_x = e_{14}\varepsilon_{yy} + \chi_{11}E_z \\ D_y &= e_{14}\varepsilon_{xz} + \chi_{11}E_y, \quad D_z = e_{14}\varepsilon_{xy} + \chi_{33}E_z \end{aligned} \quad (2)$$

**2.2. Quantum part.** Classical properties in low dimensional nanostructures are intrinsically intertwined with quantum (electronic) properties. The quantum mechanical part of our model, which we next use for simulating CdTe/ZnTe QWRs, is based on the Schrödinger equation for single conduction band. The important point to realize is that the thermopiezoelectric effects (that is classical effects described in Section 2.1) will modify the potential energy term. In our particular situation, the Schrödinger equation and effective potential are given as follows (electron is considered as a particle with effective mass  $m_e$  experiencing effective potential,  $V$ ):

$$\nabla \cdot \left\{ -\frac{\hbar^2}{2m_e} \nabla \psi \right\} + V \psi = E \psi, \quad (3)$$

$$V = r(E_x + a(\varepsilon_{xx} + \varepsilon_{yy} + \varepsilon_{zz}) - \frac{\alpha_1 T^2}{\beta_1 + T}).$$

where  $\psi$  is the wave function and  $E$  is corresponding eigenvalue,  $r$ ,  $a$ , and  $e$  are band offset ratio, conduction band deformation potential and electronic charge respectively,  $E_g$  and  $V$  are the band gap and electric potential respectively,  $\alpha_1$  and  $\beta_1$  are the Varshni coefficients [12].

The physical parameters used in this calculation are given in Table 1.

Table 1  
Physical parameters used for calculations.

Material constants	CdTe	ZnTe
$c_{11}$ (GPa)	53.8*	72.2**
$c_{12}$ (GPa)	37.4*	40.9**
$c_{44}$ (GPa)	29.18*	30.8**
$c_{12}$ (C/m <sup>2</sup> )	0.084[13]	0.028[14]
$\chi_{11}$	10.4[15]	10.3[16]
$\beta_1$ (Pa/K)	97205.65+	-73220.34+
$r$	0.75 <sup>a</sup>	0.25 <sup>b</sup>
$\alpha_1$ (eV)	-1.8 <sup>a</sup>	-3.5 <sup>a</sup>
$E_g$ (eV)	1.606 <sup>c</sup>	2.394 <sup>c</sup>
$\alpha_T$ (eV/K)	0.4357e-3[12]	0.467e-3[17]
$\beta_T$ (K)	183.31[12]	168[17]

(see [8] for notations on references and more details).

**3. Simulating quantum wire properties.** Based on the model highlighted in the previous section, we carry out simulations by using the finite element method. The domain is meshed with quadratic triangular elements and the resulting algebraic eigenvalue problem is solved numerically overcoming known difficulties [18]. A rectangular CdTe QWR of dimensions  $10 \times 10 \times 70$ nm is embedded in the  $40 \times 40 \times 150$ nm ZnTe barrier. The lattice mismatch in CdTe/ZnTe QWR is  $\epsilon_0 = 5.89\%$ .

Following [8], we recall that the magnitude of strain component  $\varepsilon_{xx}$  is observed to be less than about 3.45% ( $\sim \epsilon_0/2$ ) at all points inside the QWR, except for the region near the edges where the strain has higher magnitude than  $\epsilon_0/2$ . The QWR causes the surrounding matrix to become strained and the strain decays slowly to zero away from the QWR. We also note that the magnitude of the hydrostatic strain component is particularly important as it leads to the rigid shift in electronic band structure [19] and we refer the interested reader to [8] on particular numerical values in this case. Figure 1 shows electric potential and x-component of electric field in the x-y plane. As we pointed out in [8], the potential difference across the QWR ends is  $\sim 0.08$  V, which is smaller by order of magnitude as

compared to GaN ( $\sim 2$  V) [20]. Also, the magnitude of the electric field exceeds 5 MV/m near the edges of the QWR and has the magnitude in fractions of MV/m inside the QWR. This is again a very small magnitude of electric field as compared to GaN ( $\sim 600$  MV/m) [20].

The smaller magnitudes of electric potential and electric field represent an advantage of CdTe based nanostructures over GaN as the latter structures face a problem of higher carrier density for generating optical gain.

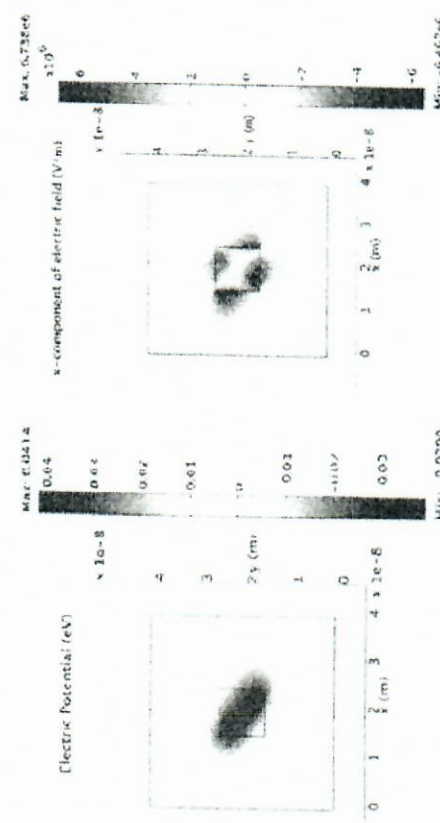


Figure 1: Electric potential (upper) and x-component of electric field in x-y plane (lower).

Figure 2 shows a)  $\varepsilon_{xx}$  along x direction and b) electric potential along Z-direction as a function of thermopiezoelectric effects. The electromechanical parameters for the CdTe/ZnTe system are relatively less sensitive to temperature than those of GaN/AlN. This can be attributed to the low values of stress-temperature coefficients and relatively weak electromechanical coupling in CdTe/ZnTe compared to the GaN/AlN system. This also provides an added advantage to CdTe/ZnTe over GaN based nanostructures related to the thermal stability of piezoelectric quantities which may result in more stable optical properties.

MV/m near the edges of the QWR and has the magnitude in fractions of MV/m inside the QWR. This is again a very small magnitude of electric field as compared to GaN ( $\sim 600$  MV/m) [20].

The smaller magnitudes of electric potential and electric field represent an advantage of CdTe based nanostructures over GaN as the latter structures face a problem of higher carrier density for generating optical gain.

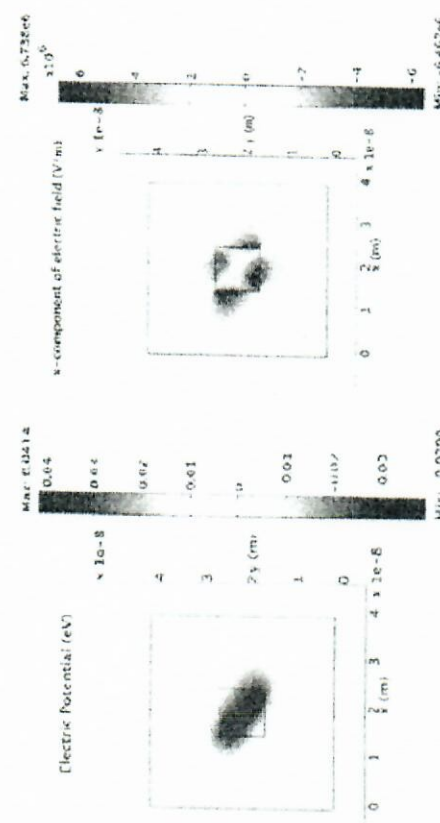


Figure 2: a)  $\varepsilon_{xx}$  and b) electric potential as a function of thermopiezoelectric effects



Figure 3: Conduction band edge shifts against thermal loadings

Figure 3 shows the conduction band edge shifts at lower temperature are positive ( $\sim 7$  meV at 0 K inside the QWR), indicating an increase in effective band gap. However, as temperature increases band gap shifts become negative ( $\sim -55$  meV at 1000 K inside the QWR). The band gap shifts range from blue shift at low temperature to red shift at higher temperatures. The band gap shifts take peak values at the edges. In the ZnTe matrix, outside the QWR, conduction band edge shifts show similar trends. The conduction band edge shift at the operating temperature of 300 K is small ( $\sim 27$  meV). Hence, we conclude that the CdTe/ZnTe QWR system is more

stable ( $\sim 1.5$  meV) than the CdTe/GaN system.

stable with respect to thermopiezoelectric effects compared to other similar materials such as GaN.

Finally, as it was pointed out in [8], the ground state eigenvalue without any electromechanical loading for CdTe/ZnTe is 0.203 eV which further decreases to 0.2025 eV and 0.197 eV with incorporation of strain and piezoelectric effects, respectively. This change in ground state eigenvalues may lead to change of optoelectronic properties.

**4. Simulating quantum dots and comparisons.** Now, we aim at comparisons of the properties of quantum nanowires and quantum dots. In this discussion, we follow closely [21] (and our recent presentation at the SPIE conference; here and further we refer to it generically as [21]). We consider cylindrical QDs and QWs which are axisymmetric around z-axis. Now we are considering a more difficult situation of wurtzite (WZ) nanostructures which have hexagonal crystallic lattice. They are axisymmetric, and therefore the solution of the model is axisymmetric as well. The material constants for the crystal with WZ symmetry used in this work are given in [21]. In this case, the original three-dimensional problem, formulated in Section 2, can be reduced to a simpler two-dimensional problem. In this case, equations (1) have the following form:

$$\frac{\partial \sigma_r}{\partial r} + \frac{\partial \sigma_z}{\partial z} + \frac{\sigma_r - \sigma_{\theta\theta}}{r} = 0, \quad \frac{\partial \sigma_r}{\partial r} + \frac{\partial \sigma_z}{\partial z} + \frac{D_r}{r} = 0. \quad (2)$$

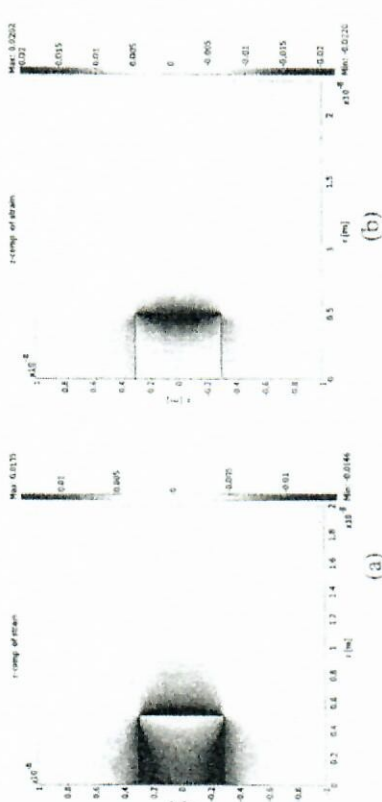
These equations are invariant with respect to rotations around the z-axis, hence solutions can be separated into a  $(r, z)$  part and a  $\theta$  part, subject to adequate boundary conditions. The constitutive relations then take the following form for WZ nanostructures:

$$\begin{aligned} \sigma_r &= C_{11}\epsilon_{rr} + C_{12}\epsilon_{\theta\theta} + C_{11}\epsilon_{zz} - e_{31}E_z - \beta_1\Theta, \quad \sigma_{rz} = C_{44}\epsilon_{rz} - e_{13}E_r, \\ \sigma_{rz} &= C_{11}\epsilon_{rr} + C_{13}\epsilon_{\theta\theta} + C_{33}\epsilon_{zz} - e_{33}E_z - \beta_3\Theta, \quad D_r = e_{13}\epsilon_{rz} - e_{11}E_r, \\ D_z &= e_{33}\epsilon_{rr} + e_{31}\epsilon_{\theta\theta} + e_{13}\epsilon_{zz} - e_{33}E_z + p_3\Theta + P_z^{SP}. \end{aligned} \quad (3)$$

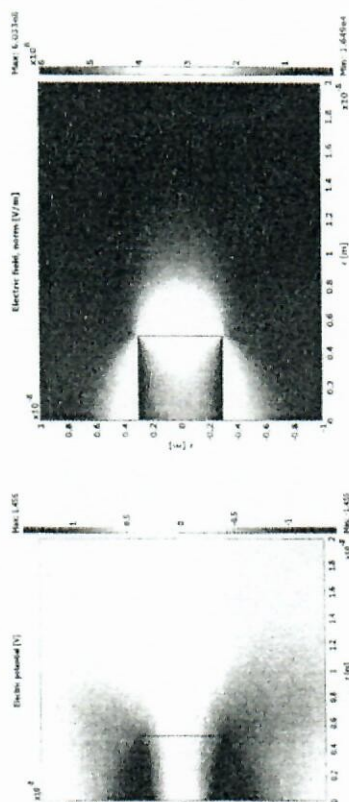
One important moment to note is that based on the total differential of the general thermodynamic potential with Taylor series expansion of differentials of electromechanical quantities a generalization of Eq. (3) to the nonlinear case can be derived [21]. To take into account the lattice mismatch by the corresponding expressions for the strain tensor components with  $\varepsilon_a = (a_m - a_Q)/a_Q$  and  $\varepsilon_c = (c_m - c_Q)/c_Q$  inside the QD and QW. Quantities  $a_m$ ,  $c_m$  and  $a_Q$ ,  $c_Q$  are the lattice constants of the matrix and the QD/QW, respectively, while quantities  $\varepsilon_a$  and  $\varepsilon_c$  are the local intrinsic strains (lattice mismatch) along the  $a$  and  $c$  directions, respectively. The directions  $a$  and  $c$  correspond to the shorter and longer dimensions of the unit cell of the wurtzite crystal, respectively. The hydrostatic strain component is given by

$$\varepsilon_{tot} = \varepsilon_{rr} + \varepsilon_{zz} + \varepsilon_{\theta\theta}$$

As we pointed out before, the hydrostatic strain component is particularly important due to the fact that it provides information about rigid shift in energy subbands. In the plane stress case, by applying a 2D analytical method, it can be defined as in [21].



(a)



(b)

Figure 4. The electromechanical distributions in QD at 300K. a) r-component of strain b) z-component of strain. c) electric potential d) electric field.

As we discussed in [21], the per cent misfit strain in the case of the GaN/AlN system is  $-2.47\%$  and  $-4.07\%$  in  $a$  and  $c$  directions, respectively. We assume that the QDs and QWs are oriented such that the  $c$ -direction of the crystal is along the  $z$ -axis. As the substrate is relatively large compared to the QD, we follow common practice to neglect lattice mismatch inside the matrix. The electromechanical parameters used in the calculations are given in [21]. All our numerical experiments have been performed under the condition for the relative errors between successive refinements to be less than  $10^{-7}$ . In our case it has been

achieved with around  $10^6$  triangular elements. Numerical solutions reflect the effect of the decreasing computational error when the solution approaches the boundary of the domain. Results originally obtained based on the development stemming from [21] clearly depict this feature, as highlighted in Figures 4, 5, and 6.

The focus we give here is on WZ GaN/AlN QD systems. Dirichlet boundary conditions are imposed along three boundaries, while other conditions are taken the same as we took earlier (see the above quoted papers). In this case, due to the axisymmetry of the system (equations, geometry and boundary conditions) there is no angular dependence. In what follows, we highlight results of [21] for the QD is of radius 5 nm and of height 10 nm and the QW is 2 micron long and has radius of 100 nm.

Figure 5 shows the electromechanical distributions in QW at 300K. Fig. 5(a) and 5(b) show distributions of  $\varepsilon_{rr}$  and  $\varepsilon_{zz}$  in  $r$ - $z$  plane, respectively. In contrast to the QD  $\varepsilon_{rr}$  has its lowest magnitude at the centre of the QW and  $\varepsilon_{zz}$  has it at the centre. Due to relatively large structure, significant strain relaxation occurs over most of the wire area. However, the electric potential (Fig. 5c), develops across the top and bottom of the QD,i.e. along  $z$ -direction. As a result of this, electric field is seen to have lowest magnitude at the centre of the QD dn has higher magnitudes near the top and bottom edges. The highest magnitude of electric field is slightly higher than that of QD, i.e.  $\sim 6.6 \times 10^8$  V/m. Our results agree well with previous reports (see [21] and references therein).

Figure 5 shows the electromechanical distributions in QW at 300K. Fig. 5(a) and 5(b) show distributions of  $\varepsilon_{rr}$  and  $\varepsilon_{zz}$  in  $r$ - $z$  plane, respectively. In contrast to the QD  $\varepsilon_{rr}$  has its lowest magnitude at the centre of the QW and  $\varepsilon_{zz}$  has it at the centre. Due to relatively large structure, significant strain relaxation occurs over most of the wire area. However, the electric potential (Fig. 5c), develops across the top and bottom of the QD,i.e. along  $z$ -direction. As a result of this, electric field is seen to have lowest magnitude at the centre of the QD dn has higher magnitudes near the top and bottom edges. The highest magnitude of electric field is slightly higher than that of QD, i.e.  $\sim 6.6 \times 10^8$  V/m. Our results agree well with previous reports (see [21] and references therein).

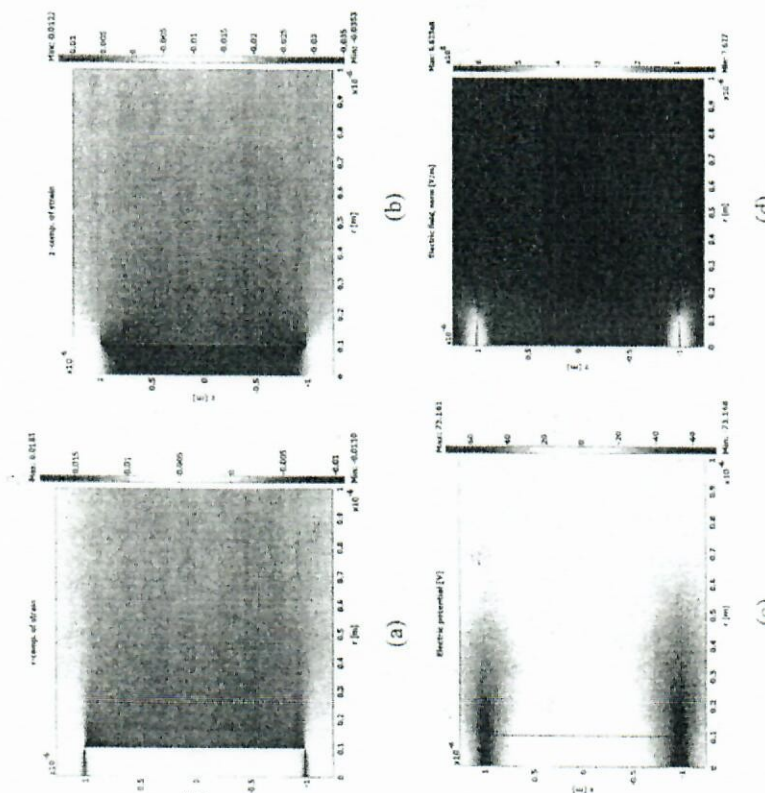


Figure 5: The electromechanical distributions in QW at 300K. a) electric potential d) electric field  
strain b) z-component of strain, c) electric potential d) electric field

Figure 4 shows the electromechanical distributions in QD at 300K. Fig. 4 a) and 4 b) show distributions of  $\varepsilon_{rr}$  and  $\varepsilon_{zz}$  in  $r$ - $z$  plane, respectively. The magnitude of both the strain components,  $\varepsilon_{rr}$  and  $\varepsilon_{zz}$ , is observed to be less than about 1% and



Figure 6 shows the effect of temperature on electromechanical quantities for the cylindrical GaN/AlN QDs. Inside the QD, the magnitude of  $\varepsilon_{rr}$  (along the  $z$ -axis at  $r = 0$ , figure 6(a)) decreases with an increase in temperature. At the center of the QD the magnitudes are  $\sim 0.8\%$  at 300 K and  $\sim 0.6\%$  at 700 K. The magnitude of  $\varepsilon_{zz}$  decreases towards zero (unstrained region) faster at higher temperature than at lower temperature. As seen from figure 6(b),  $\varepsilon_{zz}$  is negative everywhere for all temperatures. The magnitude of  $\varepsilon_{zz}$  at the centre of the QD, i.e. at  $z = 0$ , is  $\sim 0.67\%$  at 300 K, which increases with an increase in temperature to  $\sim 0.85\%$  at 700 K.

Note that as it was observed in [21], the potential difference across the top and bottom of the QD decreases with an increase in temperature, from 2.9 V at 300 K to 2.8 V at 700 K. These and other results at 300 K are in excellent agreement with theoretical and experimental reports (see [21] and references therein).

Table 1.  
Electromechanical parameters values in QD and QW at 300K at  $r=z=0$ .

	QD				QWR			
	300K	700K	300K	700K	300K	700K	300K	700K
r-comp. of strain [%]	0.8	0.6	0.7	0.8				
z-comp. of strain [%]	0.67	0.85	0.35	0.34				
Electric field [ $\times 10^4$ V/m]	4.5	4.7	0.25	0.25				

Recently we compile a table, presented at the SPIE, which we highlight here. From Table 1, it can be seen that electromechanical parameters are less sensitive in the case of QWs as compared to QD. This is due to the large area available for electromechanical relaxation. Hence, we conclude that the QW system is more stable with respect to thermopiezoelectric effects compared to QD. An order of magnitude smaller electric field observed in QWs as compared to QD, signifies that the QWs will require less amount of carrier concentration in order to generate optical gain. The smaller magnitudes of electric potential and electric field represent an advantage of CdTe/ZnTe based nanostructures over GaN as the latter structures face a problem of higher carrier density for generating optical gain [2].

**3 Conclusions.** In this contribution, we discussed the applications of a fully coupled model consisting of two parts, classical and quantum mechanical. We surveyed recent results in two areas. First, we applied our model for simulating CdTe/ZnTe quantum wires accounting for thermo-electromechanical properties. Our observations led us to conclude that thermally less sensitive electromechanical properties of CdTe/ZnTe may lead to thermally more stable performance which is important in preserving superior optoelectronic properties of nanostructures. The influence of thermal loadings on electromechanical properties of LDSNs was analyzed in detail for both two wide classes of low dimensional nanostructures, quantum wires and quantum dots. The latter has been our second area of focus. We demonstrated and emphasized that the electromechanical properties vary noticeably with temperature. In addition, we pointed out QDs are relatively more sensitive to the temperature as compared to the QWs. An order of magnitude smaller electric field observed in QWs as compared to QD, signifies that the QWs will require less amount of carrier concentration in order to generate optical gain. The results indicate that QWs have advantages over their QD counterparts, in particular with respect to the carrier density in generating optical gain. Thermally less sensitive electromechanical properties of CdTe/ZnTe may lead to thermally

more stable performance which is important in preserving superior optoelectronic properties of nanostructures.

**Acknowledgements** This work, conducted in the M<sup>3</sup>N<sub>ET</sub> Laboratory (<http://www.m3netlab.wlu.ca>), was made possible by the facilities of the SHARCNET.

1. J.T. Woo *et al.*, Strain distributions and electronic subband energies of self-assembled CdTe quantum wires grown on ZnTe buffer layers. *J. Appl. Phys.* - 2007 - 102 - Art. 033521
2. F. Bernardini, V. Fiorentini and D. Landolt, Spontaneous polarization and piezoelectric constants of III-V nitrides. *Phys. Rev. B* - 1997 - 56 - pp. 19024-19027.
3. M. Willatzen *et al.*, Dynamic coupling of piezoelectric effects, spontaneous polarization, and strain in lattice-mismatched semiconductor quantum-well heterostructures. *J. Appl. Phys.* - 2006 - 100 - Art. 024302
4. M. V. Makarov *et al.*, Calculation of the size-quantization levels in strained ZnCdSe/ZnSe quantum wells. *Semiconductors* - 1997 - 31 - pp. 800-803.
5. C. Onodera, T. Shioji, Y. Hiraiwa and T. Taguchi, Effect in changes of conduction and valence band offsets on exciton binding energy in Cd<sub>x</sub>Zn<sub>1-x</sub>Se/Zn<sub>y</sub>Se<sub>1-y</sub> single quantum wells. *Jpn. J. Appl. Phys.* - 2007 - 46 - pp. 248-250.
6. T.W. Kim *et al.*, Formation and electron activation energy of self-assembled CdTe quantum wires grown on ZnTe buffer layers. *Appl. Phys. Lett.* - 2003 - 83 - pp. 4235-4237.
7. F. E. Onischchenko *et al.*, Optical spectroscopy of CdTe/ZnTe quantum-dot superlattices. *Physica E* - 2005 - 26 - pp. 153-157.
8. S.R. Patel and R.V.N. Melnik, Thermopiezoelectric effects on optoelectronic properties of CdTe/ZnTe quantum wires. *Physica Status Solidi (a)* - 2009 - 206 - pp. 960-964.
9. R. V. N. Melnik, Computational analysis of coupled physical fields in piezothermoelastic media. *Comput. Phys. Commun.* - 2001 - 142 - pp. 231-237.
10. R. V. N. Melnik, Modelling coupled dynamics: Piezoelectric elements under changing temperature conditions. *Int. Commun. Heat Mass Transfer* - 2003 - 30 - pp. 83-92.
11. R. Melnik and R. Mahapatra, Coupled effects in quantum dot nanostuctures with nonlinear strain and bridging modelling scales. *Comput. and Struct.* - 2007 - 85 - pp. 698-711.
12. U. Pati *et al.*, Near band gap photoreflectance studies in CdTe, CdTeV and CdTe:Ge crystals. *Mater. Sci. and Eng. B* - 1996 - 42 - pp. 297-301.
13. J. Baars and F. Sorge, Resistralien spectra of InTe and Cd<sub>x</sub>Ir<sub>1-x</sub>. *Solid State Comm.* - 1972 - 10 - pp. 875-876.
14. H. D. Riccius, Infrared lattice vibrations of zinc selenide and zinc telluride. *J. Appl. Phys.* - 1968 - 39 - pp. 4381-4382.
15. M. B. Kanoun *et al.*, Zinc-blende AlN and GaN under pressure: structural, electronic, elastic and piezoelectric properties. *Semicond. Sci. Tech.* - 2004 - 19 - pp. 1220-1231.
16. D. Berlincourt, L. R. Shiozawa, H. Jaffe, Electrostatic properties of sulfides, selenides, and tellurides of zinc and cadmium. *Physical Review* - 1963 - 129 (3) - pp. 1009-1010.

17 R. Passler et al. Temperature dependence of exciton peak energies in ZnS, ZnSe, and ZnTe epitaxial films. *J. Appl. Phys.* – 1999 – 86 – pp 4403–4411.

18 R. V. N. Melnik. Topological analysis of eigenvalues in engineering computations. *Eng. Computations* – 2009 – 17 – pp 336–416.

19 J. R. Downes, D. A. Faux, and E. P. O'Reilly. Influence of strain relaxation on the electronic properties of buried quantum wells and wires. *Mater. Sci. and Eng., B* – 1995 – 35 – pp. 357–363.  
20 D. P. Williams, A. D. Andreiev and E. P. O'Reilly. Dependence of exciton energy on dot size in GaN/AlN quantum dots. *Phys. Rev., B* – 2006 – 73 – Art. 241301.  
21. S.R. Paul and R.V.N. Melnik. Thermoelastomechanical effects in quantum dots. *Nanotechnology* – 2009 – 12 – Art. 125402.

Ahc M., Msc. ScT, TUC, Porsgrunn; Lie B., Prof.Dr, TUC, Porsgrunn; Hauge T. A., Ass. Prof. Xstrata Nikkeiverk, UoA, Kristiansand;

## DYNAMIC MODELING AND VERIFICATION OF A Cu/Ni FLUIDIZED-BED ROASTER

**Abstract.** As one of the most important part of a pyrometallurgical process line, roasters represent a challenging section to optimize and control. The present work focuses on the development of the model that is depicting a transient behavior of the roaster (Fig. 1). In this particular study, the roaster behaves as a non-catalytic gas-solid reactor (NCGSR) that has characteristics of a circulating fluidized bed and of a splashing-liquid fluidized bed. Even though the real system might contain three phases, the developed model of the roaster belongs to the group of two-phase (gas and particles) models with included effects of fast water vaporization and appropriate chemical kinetics. For the modeling of the system, a set of differential algebraic equations describing the mass and energy balance is developed. The predictions of the model are compared against the temperature and concentration measurements of the real system of Xstrata Kristiansand. The model is to be further studied for optimization and model predictive control of the metallurgical plant.

**Introduction.** Term pyrometallurgy refers to the thermal treatment of metal ores and minerals, causing physical and chemical transformations of the material with the purpose of recovering desired metals. There are a number of processes considered to be pyrometallurgical, among which are: drying, calcining, roasting, smelting and refining. This paper focuses on the roasting process which is described by a non-isothermal gas-solid non-catalytic reactions. Interest is narrowed to the process of oxidation of metal ores and minerals. The oxidation or commonly called roasting reaction is hosted in a chemical reactor called fluidized-bed roaster. Although non-catalytic gas-solid reactions have been studied extensively in the past [6], a general framework for modeling a non-catalytic

fluidized-bed reactor has not been yet fully formulated. An attempt to give such a general formulation is made in [7], where the developed approach was applied to char coal gasification process. An extensive steady state analysis on the theoretical and practical basis for catalytic and non-catalytic reactors is given in [1]. With the focus on engineering applications, it provides a good reference for finding reaction rate and supported analytical solutions to the problem of finding reaction rate and conversion times, among many other design parameters. Dynamic modeling of the entire roasting plant and accompanied cleaning system along with some studies of the control strategy are given in [2, 3]. Some examples of modeling the similar problems are given in [4, 8]. Nevertheless, the specific design of the fluidized-bed roaster in this paper makes it unique in the sense that not much previous work is available (published), especially for the industrial scale conditions. Need for an application of advanced control strategies has been the main motivator to find a simple and robust dynamic model.

**Process description.** The roasting process is hosted in a closed circulating fluidized-bed reactor (CFB) vessel called the roaster (Fig. 1a). The system in reality operates with three phases: gas, solid and liquid. The fluidizing gas enters the system from the bottom of the bed in the form of bubbles, stirring the solid phase. A mixture of water and solids, slurry, is dispersed from the top of the vessel into the freeboard. Inside the freeboard mixture is contacted with the up-flowing stream of gas, exchanging heat and mass. The water is evaporated due to high temperatures, and the solid particles are partially chemically transformed (converted) by the combustion reaction. The solids inside the freeboard travel in two directions, one stream flows towards the off-gas exit carried by the gas, and another stream settles on the surface of the bed. In practice, parameters like particles size distribution, subsequent fan suction and outlet design, determine the flow rate of each stream.

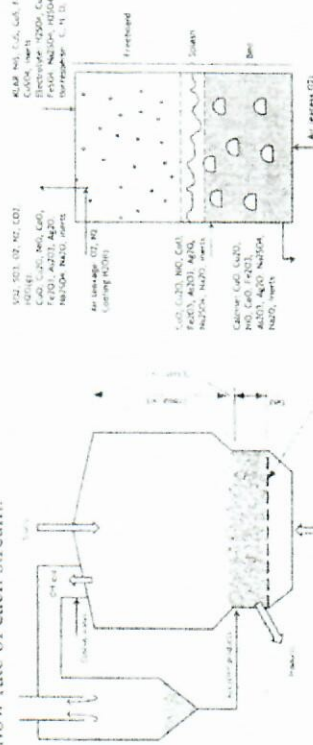


Fig. 1. a) Roaster b) Species in the system

The carried-over particles are captured by the cyclone and recirculated into the bed. Products of the conversion inside the roaster are taken out mostly from the bed zone and a certain amount of solids is joined from the recirculated cyclone

## **MODELING-2010 / SIMULATION-2010**

**Chair of the Organizing Committee: Professor O. A. Chemerys**  
**Chair of the Program Committee: Professor V. F. Evdokimov**

### **OBJECTIVES AND TOPICS**

The purpose of the conference is strengthening and development of scientific and technical collaboration of specialists in area of mathematical modeling and computer simulation in different branches of science, technique, industry and economy.

The main themes of the conference center around modern problems of mathematical and computer modeling and include the following topics:

- theory of mathematical modeling and computer simulation
- numerical methods and high-performance computing
- the applied methods of mathematical modeling and computer simulation in the different areas of activity (in science, energy engineering, economy, ecology, management, and other areas)
- application of parallel computing and new information technologies for solving problems of mathematical modeling and computer simulation
- cybersecurity and information security systems
- advanced computer systems in simulation and training.

**Publication of the Georgy Pukhov NASU Institute for Energy Modeling**